INSTITUTE OF PHYSICS PUBLISHING COMBUSTION THEORY AND MODELLING

Combust. Theory Modelling **8** (2004) 683–699 PII: S1364-7830(04)69840-8

# The effect of heat loss on flame edges in a non-premixed counterflow within a thermo-diffusive model

**R Daou, J Daou and J Dold**

Department of Mathematics MIST, Manchester M60 1QD, UK

Received 2 October 2003, in final form 28 April 2004
Published 19 July 2004
Online at stacks.iop.org/CTM/8/683
doi:10.1088/1364-7830/8/4/002

**Abstract**

We present an asymptotic study of the effect of volumetric heat loss on the propagation of triple flames in a counterflow configuration at constant density. Analytical results for the speed, the local burning rate, the shape and the extent of the flame front are derived in the asymptotic limits of weak strain rates and large activation energies and for Lewis numbers that are near unity. The results account for the combined effects of strain, heat loss, composition gradients and non-unit Lewis numbers and provide Markstein-type relationships between the local burning speed (or local flame temperature) and the local flame stretch and can be useful for future investigations in deriving such relationships in non-homogeneous non-adiabatic mixtures under more general flow conditions. The analytical predictions are complemented by and compared with numerical predictions focusing on the low strain regime and allowing for non-unit Lewis numbers. The numerical findings are found to be in good qualitative agreement with the asymptotics, both in predicting extinction (e.g. as the burning leading-front of a triple flame becomes vanishingly small) and in the dependence of the propagation speed on heat loss, strain and the Lewis numbers. Quantitative discrepancies are discussed and are found to be mainly attributable to the infinite activation energy assumption used in the asymptotics.

## 1. Introduction

The role of triple flames as a fundamental structure in combustion applications is now well established, involving phenomena such as flame spread in mixing layers, flame spread over solid or liquid fuel surfaces, ignition and extinction of diffusion flames and flame stabilization in reactive streams. Several aspects of the problem have been studied since the early work of Phillips [1], Ohki and Tsuge [2] and Dold and collaborators [3, 4]. These include the effect of gas expansion, the influence of non-unit Lewis numbers and the stability of triple flames (see [5–11] and references therein).

  

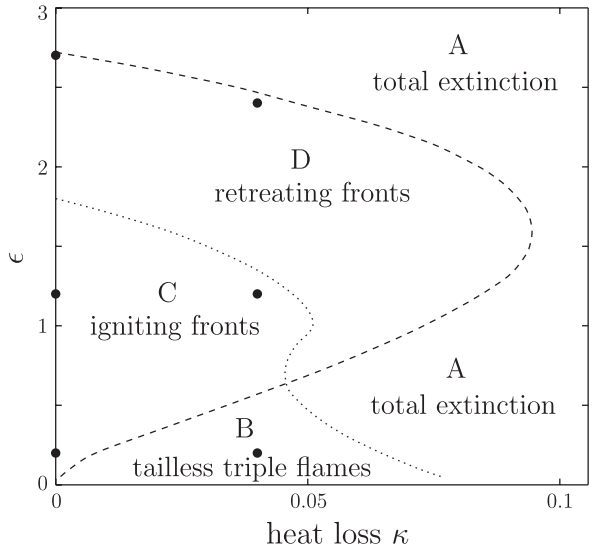


**Figure 1.** Regimes of triple flame propagation in a strained flow with heat loss at unit Lewis numbers. The dimensionless strain rate is measured by $\epsilon$ and the rate of heat loss by $\kappa$. The dark circles mark the parameter values used for calculating the triple flame structures shown in figure 2.

However, an important aspect of the problem that has received little attention, at least as far as the prototypical counterflow configuration is concerned, is the effect of volumetric heat loss. Kurdyumov and Matalon [12] found numerical evidence that heat loss can be responsible for triple flame oscillations in a non-strained mixing layer. An asymptotic and numerical study of the effect of heat loss on flame edges in a premixed counterflow [13] has revealed a wide range of possible forms of behaviour.

In considering a non-premixed counterflow geometry with Lewis numbers of unity, another recent numerical study [14] has revealed the different forms of behaviour that are adopted by triple flames at different levels of heat loss and strain rate. These are illustrated in figures 1 and 2. As should be expected, with excessive strain or excessive heat loss there is no burning at all (region A of figure 1), and with no heat loss the speed of propagation of the triple flame changes from being positive (region C) to negative (region D) as the strain rate is increased. However, when there is heat loss a new phenomenon arises at relatively low strain rates: even with very small rates of heat loss the diffusion flame is quenched at small enough values of the strain rate, although the premixed flame branches of the triple flame continue to survive and propagate (see the top left diagram of figure 2). The phenomenon persists at higher rates of heat loss, provided these are not too high.

In fact, such a flame structure can be thought of as a flame edge that survives even though the flame to which it might otherwise have been attached is extinguished; the term 'edge flame' may then be more appropriate in this case. There are non-burning conditions both ahead of it and behind it. At small enough rates of heat loss, these tailless triple flames (region B) lose their structure by recreating a diffusion flame in their wake as the strain rate is increased. On the other hand, at higher rates of heat loss they are quenched completely as the strain rate is increased, before any diffusion flame can be reestablished. The natural divisions between all these regions are the dashed line in figure 1 where a planar diffusion flame quenches and the dotted line at which the propagation speed of the triple flame, with or without a trailing diffusion flame, becomes zero. These findings are all based on calculations at unit Lewis numbers [14].

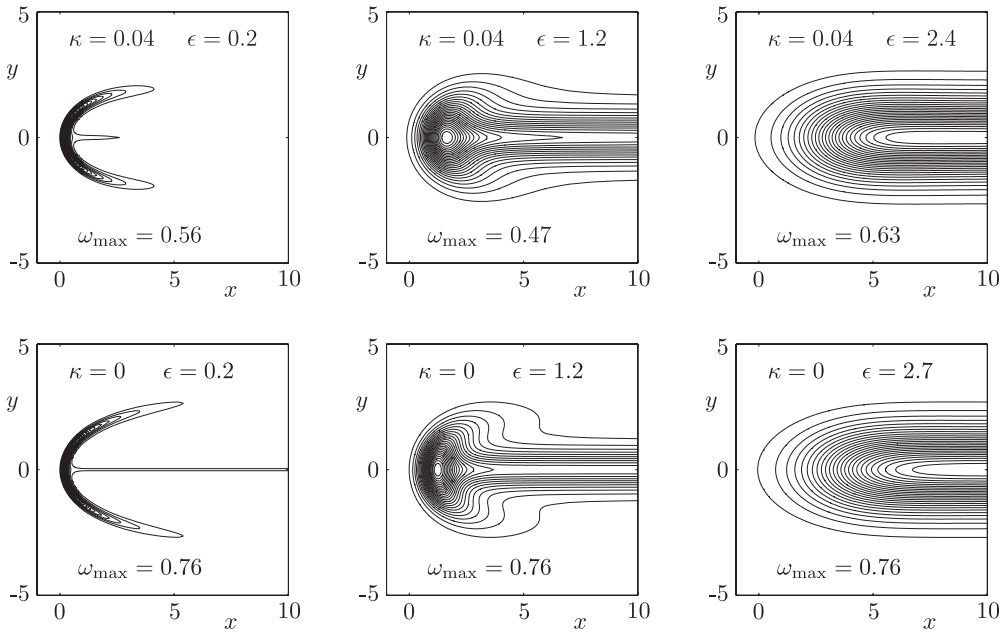


**Figure 2.** Reaction-rate contours with no heat loss (lower subfigures) and with $\kappa = 0.04$ (upper subfigures) at increasing dimensionless strain rates $\epsilon$.

In this paper, we help to clarify some of the underlying reasons for this range of behaviour by examining the asymptotic structure of triple flames with heat loss at small rates of strain. This is precisely the regime in which tailless triple flames appear. As well as providing asymptotic descriptions of the phenomena, the analysis reveals the effect of Lewis numbers that may be close to, but not equal to, unity. The Markstein-type relationships between the local burning speed (or local flame temperature) and the local flame stretch derived in the present counterflow configuration can be viewed as an important first step for deriving such relationships in non-homogeneous non-adiabatic mixtures under more general flows. We also present further, numerical results to complement the asymptotic findings, particularly at non-unit Lewis numbers.

This paper is structured as follows. The problem is first formulated in the context of the thermo-diffusive approximation for which density and transport properties are constant, with a single Arrhenius reaction. An asymptotic analysis in the limits of large activation temperature and weak strain rate is then carried out. This is followed by a numerical examination, including a comparison with the asymptotic results.

## 2. Formulation

A useful flow configuration in which to study triple flames is a two-dimensional counterflow, as illustrated in figure 3, with an inflow of $v_Y = -aY$ in the $Y$-direction and an outflow of $v_Z = aZ$ in the $Z$-direction (with $a$ denoting the strain rate). The flow in the $X$-direction is fixed at zero, $v_X = 0$. The upper incoming flow can be considered to deliver an oxidizer while the lower flow delivers fuel that can mix and react in the resulting mixing layer.

We consider steady propagation of two-dimensional triple flames in this layer (being uniform in the $Z$-direction) with propagation speed $\hat{U}$ in the negative direction along the

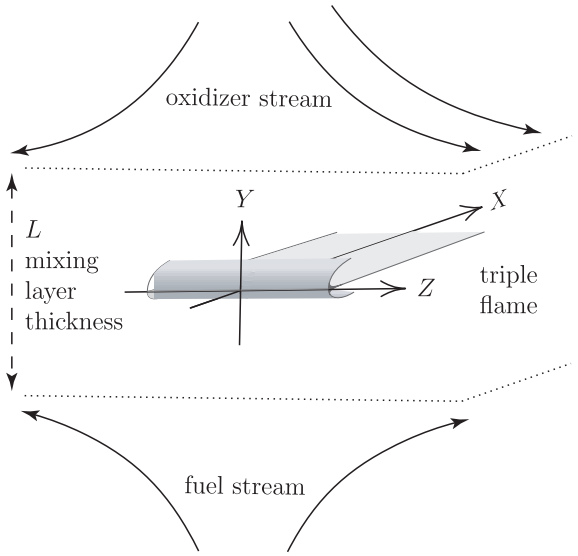


**Figure 3.** Schematic illustration of a triple flame in a counterflow configuration.

$X$-axis. A single one-step reaction, $\mathrm{F} + s\mathrm{Ox} \rightarrow \mathrm{P} + q$, is assumed, where F denotes the fuel, Ox the oxidizer and P the products. The quantities $s$ and $q$ represent the mass of oxidizer consumed and the heat released per unit mass of fuel. The reaction rate, $\hat{\omega}$, is taken to follow an Arrhenius Law of the form $\hat{\omega} = B\rho^2 Y_\mathrm{F} Y_\mathrm{O} \exp(-E/RT)$, where $B$, $\rho$, $Y_\mathrm{F}$, $Y_\mathrm{O}$ and $E/R$ are the pre-exponential factor, density, mass fractions of fuel and oxidizer and the activation temperature, respectively. In a reference frame that follows a steadily propagating flame, the governing equations are

$$\hat{U}\frac{\partial T}{\partial X} = D_\mathrm{T}\left(\frac{\partial^2 T}{\partial X^2} + \frac{\partial^2 T}{\partial Y^2}\right) + \frac{q}{c_\mathrm{p}}\frac{\hat{\omega}}{\rho} + aY\frac{\partial T}{\partial Y} - \hat{\kappa}(T - T_0), \tag{1}$$

$$\hat{U}\frac{\partial Y_\mathrm{F}}{\partial X} = D_\mathrm{F}\left(\frac{\partial^2 Y_\mathrm{F}}{\partial X^2} + \frac{\partial^2 Y_\mathrm{F}}{\partial Y^2}\right) - \frac{\hat{\omega}}{\rho} + aY\frac{\partial Y_\mathrm{F}}{\partial Y}, \tag{2}$$

$$\hat{U}\frac{\partial Y_\mathrm{O}}{\partial X} = D_\mathrm{O}\left(\frac{\partial^2 Y_\mathrm{O}}{\partial X^2} + \frac{\partial^2 Y_\mathrm{O}}{\partial Y^2}\right) - s\frac{\hat{\omega}}{\rho} + aY\frac{\partial Y_\mathrm{O}}{\partial Y}. \tag{3}$$

The diffusion coefficients $D_\mathrm{F}$, $D_\mathrm{O}$ and $D_\mathrm{T}$ of fuel, oxidant and heat are taken to be constant, as is the specific heat at constant pressure, $c_\mathrm{p}$. With $T_0$ representing the 'ambient' temperature in both incoming streams, the last term on the right-hand side of equation (1) represents a linear volumetric rate of heat loss with coefficient $\hat{\kappa}$. As boundary conditions we shall apply the planar $Y$-dependent frozen mixing layer solution as $X \rightarrow -\infty$ or $Y \rightarrow \pm\infty$ and vanishing $X$-derivatives as $X \rightarrow +\infty$.

Suitable non-dimensional dependent variables can be defined as

$$y_\mathrm{F} = \frac{Y_\mathrm{F}}{Y_{\mathrm{F,st}}}, \qquad y_\mathrm{O} = \frac{Y_\mathrm{O}}{Y_{\mathrm{O,st}}} \qquad \text{and} \qquad \theta = \frac{T - T_0}{T_\mathrm{ad} - T_0},$$

in which the subscript 'st' refers to values at $(X, Y) = (-\infty, Y_\mathrm{st})$, where $Y_\mathrm{st}$ is the location of the upstream stoichiometric surface, at which $Y_\mathrm{O} = sY_\mathrm{F}$ or

$$S\,\mathrm{erf}\left(\frac{Y_\mathrm{st}}{(2D_\mathrm{F}/a)^{1/2}}\right) + \mathrm{erf}\left(\frac{Y_\mathrm{st}}{(2D_\mathrm{O}/a)^{1/2}}\right) = S - 1. \tag{4}$$

The constant $S$ is given by $S \equiv sY_{\mathrm{F,F}}/Y_{\mathrm{O,O}}$ (taking $Y_{\mathrm{F,F}}$ and $Y_{\mathrm{O,O}}$ to denote the mass fractions of fuel and oxidant in their respective incoming streams). The adiabatic stoichiometric flame temperature is defined by $T_{\mathrm{ad}} \equiv T_0 + qY_{\mathrm{F,st}}/c_{\mathrm{p}}$. Lengths will be measured against the unit $L/\beta$, where $L \equiv (2D_{\mathrm{T}}/a)^{1/2}$ is the thermal mixing layer thickness and $\beta \equiv E(T_{\mathrm{ad}} - T_0)/RT_{\mathrm{ad}}^2$ is the Zeldovich number; the length $L/\beta$ is characteristic of the radius of curvature of a triple flame [3]. Speed will be measured against the leading order asymptotic value of the speed of a stoichiometric planar flame, for large $\beta$, under adiabatic equidiffusional conditions, namely $S_L^0 = \{4\beta^{-3}Y_{\mathrm{O,st}}\rho D_{\mathrm{T}}B\exp(-E/RT_{\mathrm{ad}})\}^{1/2}$.

Thus, defining $y \equiv \beta(Y - Y_{\mathrm{st}})/L$ and $x \equiv \beta X/L$, equations (1)–(3) take the form

$$U\frac{\partial\theta}{\partial x} = \epsilon\left(\frac{\partial^2\theta}{\partial x^2} + \frac{\partial^2\theta}{\partial y^2}\right) + \epsilon^{-1}\omega + \frac{2\epsilon}{\beta}\left(\eta_s + \frac{y}{\beta}\right)\frac{\partial\theta}{\partial y} - \frac{\epsilon^{-1}}{\beta}\kappa\theta, \tag{5}$$

$$U\frac{\partial y_{\mathrm{F}}}{\partial x} = \frac{\epsilon}{\mathrm{Le_F}}\left(\frac{\partial^2 y_{\mathrm{F}}}{\partial x^2} + \frac{\partial^2 y_{\mathrm{F}}}{\partial y^2}\right) - \epsilon^{-1}\omega + \frac{2\epsilon}{\beta}\left(\eta_s + \frac{y}{\beta}\right)\frac{\partial y_{\mathrm{F}}}{\partial y}, \tag{6}$$

$$U\frac{\partial y_{\mathrm{O}}}{\partial x} = \frac{\epsilon}{\mathrm{Le_O}}\left(\frac{\partial^2 y_{\mathrm{O}}}{\partial x^2} + \frac{\partial^2 y_{\mathrm{O}}}{\partial y^2}\right) - \epsilon^{-1}\omega + \frac{2\epsilon}{\beta}\left(\eta_s + \frac{y}{\beta}\right)\frac{\partial y_{\mathrm{O}}}{\partial y}, \tag{7}$$

in which we define

$$\epsilon \equiv \frac{\ell_{\mathrm{fl}}^0}{L/\beta} \equiv \frac{\beta(D_{\mathrm{T}}/2)^{1/2}}{S_L^0}a^{1/2},$$

which represents the dimensionless thickness of a laminar stoichiometric flame (dimensionally $\ell_{\mathrm{fl}}^0 = D_{\mathrm{T}}/S_L^0$); it also varies as the square root of the strain rate. Lewis numbers of fuel and oxidizer are $\mathrm{Le_F} \equiv D_{\mathrm{T}}/D_{\mathrm{F}}$ and $\mathrm{Le_O} \equiv D_{\mathrm{T}}/D_{\mathrm{O}}$. The parameter $\eta_s \equiv Y_{\mathrm{st}}/\{2D_{\mathrm{T}}/a\}^{1/2}$ provides the dimensionless location of the upstream stoichiometric surface ($y = \eta_s$), for which the dimensionless form of (4),

$$S\,\mathrm{erf}(\eta_s\mathrm{Le_F^{1/2}}) + \mathrm{erf}(\eta_s\mathrm{Le_O^{1/2}}) = S - 1,$$

relates $S$ and $\eta_s$. The dimensionless coefficient $\kappa \equiv \beta(D_{\mathrm{T}}/S_L^{0\,2})\hat{\kappa}$ now parametrizes the rate of heat loss, and the dimensionless reaction rate, $\omega$, is given by

$$\omega \equiv \frac{\beta^3}{4}y_{\mathrm{F}}y_{\mathrm{O}}\exp\frac{\beta(\theta - 1)}{1 + \alpha_h(\theta - 1)} \tag{8}$$

with $\alpha_h \equiv (T_{\mathrm{ad}} - T_0)/T_{\mathrm{ad}}$.

In terms of the new variables, the boundary conditions, as $x \to -\infty$ or $y \to \pm\infty$, are

$$\begin{aligned}
&\theta = 0,\\
&y_{\mathrm{F}} = \frac{1 - \mathrm{erf}\,[(\eta_s + y/\beta)\mathrm{Le_F^{1/2}}]}{1 - \mathrm{erf}(\eta_s\mathrm{Le_F^{1/2}})},\\
&y_{\mathrm{O}} = \frac{1 + \mathrm{erf}\,[(\eta_s + y/\beta)\mathrm{Le_O^{1/2}}]}{1 + \mathrm{erf}(\eta_s\mathrm{Le_O^{1/2}})}
\end{aligned} \tag{9}$$

and as $x \to +\infty$ we impose the conditions

$$\frac{\partial\theta}{\partial x} = \frac{\partial y_{\mathrm{F}}}{\partial x} = \frac{\partial y_{\mathrm{O}}}{\partial x} = 0. \tag{10}$$

These equations can be used to determine the relationship between the dimensionless propagation speed, $U$, and the parameters, $\epsilon$, $\kappa$, $\mathrm{Le_F}$, $\mathrm{Le_O}$ and $\eta_s$ (in addition to $\beta$ and $\alpha_h$). In particular, we seek to find an asymptotic expression (in the next section) with which to study the influence of heat loss and strain rate (characterized by $\epsilon$ and $\kappa$) on triple flame propagation for Lewis numbers that are close to unity.

## 3. The weak strain asymptotic limit

In this section, as in [9], we begin by, first, reformulating the problem in the asymptotic limit $\beta \to \infty$ with $\epsilon = \mathrm{O}(1)$, in the context of the nearly equidiffusive approximation, for which $l_\mathrm{F} \equiv \beta(\mathrm{Le_F} - 1)$ and $l_\mathrm{O} \equiv \beta(\mathrm{Le_O} - 1)$ are of order unity. In the reformulated problem thus obtained, now independent of $\beta$, we then consider the limit $\epsilon \to 0$. The results are then expected to be valid, provided the activation energy is large and the strain rate is small, more precisely, for $\beta^{-1} \ll \epsilon \ll 1$.

In the limit $\beta \to \infty$, the reaction zone is confined to an infinitely thin region or flame sheet located on a path represented by $x = f(y)$ say, and the upstream boundary conditions (9) can be linearized to give

$$\theta = 0, \qquad y_\mathrm{F} = 1 - \frac{\gamma_\mathrm{F}}{\beta} y, \qquad y_\mathrm{O} = 1 + \frac{\gamma_\mathrm{O}}{\beta} y, \tag{11}$$

in the flame front region, where $y = \mathrm{O}(1)$. The constants $\gamma_\mathrm{F}$, $\gamma_\mathrm{O}$ are given by

$$\gamma_\mathrm{F} = \frac{2\exp(-\eta_s^2)}{\sqrt{\pi}(1 - \mathrm{erf}(\eta_s))}, \qquad \gamma_\mathrm{O} = \frac{2\exp(-\eta_s^2)}{\sqrt{\pi}(1 + \mathrm{erf}(\eta_s))} \tag{12}$$

and can be expressed in terms of the stoichiometric parameter, $S$, using

$$\eta_s = \mathrm{erf}^{-1}\left(\frac{S-1}{S+1}\right), \tag{13}$$

provided $l_\mathrm{F}$ and $l_\mathrm{O}$ are order one (the nearly equidiffusive limit).

We shall use expansions in terms of $\beta^{-1}$ of the form

$$y_\mathrm{F} = y_\mathrm{F}^0 + \beta^{-1} y_\mathrm{F}^1 + \cdots, \qquad y_\mathrm{O} = y_\mathrm{O}^0 + \beta^{-1} y_\mathrm{O}^1 + \cdots, \qquad \theta = \theta^0 + \beta^{-1}\theta^1 + \cdots.$$

Then, given that the heat loss term in (5) and the gradients in the upstream boundary conditions (11) are of order $\beta^{-1}$, we have $\theta^0 + y_\mathrm{F}^0 = 1$ and $\theta^0 + y_\mathrm{O}^0 = 1$, identically, and

$$\theta^0 = 1, \quad y_\mathrm{F}^0 = 0, \quad y_\mathrm{O}^0 = 0 \qquad \text{in the burnt gas.} \tag{14}$$

In terms of $\theta^0$ and the excess enthalpies $h \equiv \theta^1 + y_\mathrm{F}^1$ and $k \equiv \theta^1 + y_\mathrm{O}^1$, the governing equations yield

$$U\frac{\partial \theta^0}{\partial \xi} = \epsilon \Delta \theta^0, \tag{15}$$

$$U\frac{\partial h}{\partial \xi} = \epsilon \Delta h + \epsilon l_\mathrm{F} \Delta \theta^0 - \epsilon^{-1}\kappa\theta^0, \tag{16}$$

$$U\frac{\partial k}{\partial \xi} = \epsilon \Delta k + \epsilon l_\mathrm{O} \Delta \theta^0 - \epsilon^{-1}\kappa\theta^0, \tag{17}$$

to be solved on both sides of the reaction sheet where $\xi \equiv x - f(y) \neq 0$, subject to the jump conditions

$$\begin{aligned} &[\theta^0] = [h] = [k] = 0, \\ &\left[\frac{\partial h}{\partial \xi}\right] = -l_\mathrm{F}\left[\frac{\partial \theta^0}{\partial \xi}\right], \qquad \left[\frac{\partial k}{\partial \xi}\right] = -l_\mathrm{O}\left[\frac{\partial \theta^0}{\partial \xi}\right], \\ &\epsilon\sqrt{1+f'^2}\left[\frac{\partial \theta^0}{\partial \xi}\right] = -\left(1 + \frac{\mu - \sigma}{2}\right)^{1/2} \exp\left(\frac{\sigma}{2}\right) \end{aligned} \tag{18}$$

at $\xi = 0$. This is a standard reduction of the problem in the limit $\beta \to \infty$ [9]. Here, $[\psi] \equiv \psi(\xi = 0^+, y) - \psi(\xi = 0^-, y)$ indicates the jump of any quantity $\psi$, and the notation

$$\begin{cases} \sigma = h(0^+, y), \quad \mu = k(0^+, y) & \text{(fuel-lean side } k \geqslant h), \\ \sigma = k(0^+, y), \quad \mu = h(0^+, y) & \text{(fuel-rich side } k < h), \end{cases} \tag{19}$$

has been used, so that $\mu - \sigma$ is never negative. In addition, the upstream boundary conditions, which follow from (11), are

$$\theta^0 = 0, \quad h = -\gamma_F y, \quad k = \gamma_O y \qquad \text{as } \xi \to -\infty. \tag{20}$$

These can also be used for finite values of $\xi$ and $|y| \to \infty$ since they are exact solutions of (15)–(18). As conditions in the burnt gas, we shall simply require that $\theta^0 = 1$ and that the solutions are free from exponentially growing terms as $\xi \to \infty$.

### *3.1. Expansions for $\epsilon \ll 1$*

In the limit $\epsilon \to 0$, the flame, including its preheat zone, can be viewed as an infinitely thin layer located at $\xi = 0$ since its thickness is $O(\epsilon)$. We shall write expansions in the form

$$f = f_0 + \epsilon f_1 + \cdots, \qquad U = U_0 + \epsilon U_1 + \cdots$$

with similar expressions for $\theta$, $h$ and $k$ written for the different regions. We begin by seeking outer expansions in the form

$$\theta^0 = \Theta_0 + \epsilon\Theta_1 + \cdots, \qquad h = H_0 + \epsilon H_1 + \cdots, \qquad k = K_0 + \epsilon K_1 + \cdots$$

on both sides of the flame, $\xi < 0$ and $\xi > 0$, which we substitute into equations (15)–(17). For $\theta^0$ we find, taking into account the boundary conditions as $\xi \to \pm\infty$,

$$\theta^0 = \Theta_0 = \begin{cases} 0 & \text{for } \xi < 0, \\ 1 & \text{for } \xi > 0, \end{cases} \qquad \Theta_1 = \Theta_2 = \cdots = 0. \tag{21}$$

Then, from $U_0 \partial H_0/\partial\xi = U_0 \partial K_0/\partial\xi = -\epsilon^{-1}\kappa\Theta_0$ and the upstream boundary conditions (20), it follows that

$$H_0 = \begin{cases} -\gamma_F y & \text{for } \xi < 0, \\ -\left(\dfrac{\kappa}{\epsilon U_0}\right)\xi + A & \text{for } \xi > 0 \end{cases} \tag{22}$$

and

$$K_0 = \begin{cases} \gamma_O y & \text{for } \xi < 0, \\ -\left(\dfrac{\kappa}{\epsilon U_0}\right)\xi + B & \text{for } \xi > 0, \end{cases} \tag{23}$$

where $A$ and $B$ are functions of integration that may depend on $y$. We note that $H_1 = H_2 = \cdots = 0$ and $K_1 = K_2 = \cdots = 0$ for $\xi < 0$, as can be checked.

### *3.2. The inner expansion and the solution to leading order*

Using the stretched variable $\zeta \equiv \xi/\epsilon$, we write inner expansions in the form

$$\theta^0 = \theta_0 + \epsilon\theta_1 + \cdots, \qquad h = h_0 + \epsilon h_1 + \cdots, \qquad k = k_0 + \epsilon k_1 + \cdots.$$

In terms of $\zeta$ the leading order equations in the inner region are

$$U_0 \frac{\partial\theta_0}{\partial\zeta} = (1 + f_0'^2)\frac{\partial^2\theta_0}{\partial\zeta^2}, \tag{24}$$

$$U_0 \frac{\partial h_0}{\partial\zeta} = (1 + f_0'^2)\frac{\partial^2 h_0}{\partial\zeta^2} + l_F(1 + f_0'^2)\frac{\partial^2\theta_0}{\partial\zeta^2} - \kappa\theta_0, \tag{25}$$

$$U_0 \frac{\partial k_0}{\partial\zeta} = (1 + f_0'^2)\frac{\partial^2 k_0}{\partial\zeta^2} + l_O(1 + f_0'^2)\frac{\partial^2\theta_0}{\partial\zeta^2} - \kappa\theta_0. \tag{26}$$

These yield, when solved with the jump conditions that follow from (18) and matched with the outer solutions (21)–(23), the leading order solutions

$$\theta_0 = \begin{cases} \exp(\alpha\zeta) & \text{for } \zeta \leqslant 0, \\ 1 & \text{for } \zeta \geqslant 0, \end{cases} \tag{27}$$

$$h_0 = \begin{cases} -\gamma_F y - \left[\left(\alpha l_F - \dfrac{\kappa}{U_0}\right)\zeta + \dfrac{2\kappa}{\alpha U_0}\right]\exp(\alpha\zeta) & \text{for } \zeta \leqslant 0, \\ -\gamma_F y - \dfrac{2\kappa}{\alpha U_0} - \left(\dfrac{\kappa}{U_0}\right)\zeta & \text{for } \zeta \geqslant 0, \end{cases} \tag{28}$$

$$k_0 = \begin{cases} \gamma_O y - \left[\left(\alpha l_O - \dfrac{\kappa}{U_0}\right)\zeta + \dfrac{2\kappa}{\alpha U_0}\right]\exp(\alpha\zeta) & \text{for } \zeta \leqslant 0, \\ \gamma_O y - \dfrac{2\kappa}{\alpha U_0} - \left(\dfrac{\kappa}{U_0}\right)\zeta & \text{for } \zeta \geqslant 0, \end{cases} \tag{29}$$

where

$$\alpha \equiv \frac{U_0}{1 + f_0'^2}. \tag{30}$$

We note that, in determining $h_0$ and $k_0$ for $\zeta \geqslant 0$, we have used the fact that no exponential growth as $\zeta$ increases is allowed by the matching; completing the matching allows $A$ and $B$ to be determined in (22) and (23), namely $A = -\gamma_F y - 2\kappa/(\alpha U_0)$ and $B = \gamma_O y - 2\kappa/(\alpha U_0)$.

Now using the jump condition (18.c) together with (19) and (28)–(30) we obtain

$$\frac{U_0 \exp[\kappa(1 + f_0'^2)/U_0^2]}{(1 + f_0'^2)^{1/2}} = \bar{S}_L(y) = \begin{cases} \left(1 + \dfrac{\gamma_F + \gamma_O}{2} y\right)^{1/2} \exp\left(-\dfrac{\gamma_F y}{2}\right) & \text{for } y \geqslant 0, \\ \left(1 - \dfrac{\gamma_F + \gamma_O}{2} y\right)^{1/2} \exp\left(\dfrac{\gamma_O y}{2}\right) & \text{for } y \leqslant 0. \end{cases} \tag{31}$$

With $\bar{S}_L(y)$ denoting the function of $y$ defined by the right-hand side of (31), we thus have

$$S_{L0} \exp\left(\frac{\kappa}{S_{L0}^2}\right) = \bar{S}_L, \tag{32}$$

where

$$S_{L0} = S_{L0}(y) \equiv \frac{U_0}{(1 + f_0'^2)^{1/2}}$$

is the local laminar flame speed, to leading order. When $\kappa = 0$, we can note that $\bar{S}_L = S_{L0}$ so that $\bar{S}_L(y)$ represents the local normal propagation speed of the premixed flame branches of the *adiabatic* triple flame.

From (31), it is possible to determine the first approximation to the propagation speed, $U_0$, and to the location of the leading edge, $y^*$, say; we simply use the fact that, at $y = y^*$, $f_0' = 0$ and $S_{L0}$ is maximum. We thus find that

$$y^* = \begin{cases} \dfrac{\gamma_O - \gamma_F}{\gamma_F(\gamma_F + \gamma_O)} & \text{for } \gamma_F \leqslant \gamma_O, \\ \dfrac{\gamma_O - \gamma_F}{\gamma_O(\gamma_F + \gamma_O)} & \text{for } \gamma_F \geqslant \gamma_O \end{cases}$$

and

$$U_0 \exp\left(\frac{\kappa}{U_0^2}\right) = \begin{cases} \sqrt{\dfrac{\gamma_F + \gamma_O}{2\gamma_F}} \exp\dfrac{\gamma_F - \gamma_O}{2(\gamma_F + \gamma_O)} & \text{for } \gamma_F \leqslant \gamma_O, \\ \sqrt{\dfrac{\gamma_F + \gamma_O}{2\gamma_O}} \exp\dfrac{\gamma_O - \gamma_F}{2(\gamma_F + \gamma_O)} & \text{for } \gamma_F \geqslant \gamma_O. \end{cases}$$

These relations can be expressed in terms of the stoichiometric coefficient, $S$, using (12) and (13) as

$$y^* = \begin{cases} -\sqrt{\pi}\dfrac{S-1}{(S+1)^2}\exp\left[\mathrm{erf}^{-1}\left(\dfrac{S-1}{S+1}\right)\right]^2 & \text{for } S \leqslant 1, \\ -\sqrt{\pi}\dfrac{(S-1)S}{(S+1)^2}\exp\left[\mathrm{erf}^{-1}\left(\dfrac{S-1}{S+1}\right)\right]^2 & \text{for } S \geqslant 1 \end{cases} \tag{33}$$

and

$$U_0 \exp\left(\frac{\kappa}{U_0^2}\right) = \bar{U}_0(S) \equiv \begin{cases} \sqrt{\dfrac{S+1}{2S}}\exp\dfrac{S-1}{2(S+1)} & \text{for } S \leqslant 1, \\ \sqrt{\dfrac{S+1}{2}}\exp\dfrac{1-S}{2(S+1)} & \text{for } S \geqslant 1. \end{cases} \tag{34}$$

We note that replacing $S$ by $S^{-1}$ in (33) and (34) keeps $U_0$ unchanged while changing the sign of $y^*$. This fact should be expected from the definition of $S$ because swapping the 'labels' of the reactants as 'fuel' or 'oxidizer' does not change the underlying physical problem in any way at all.

Now the right-hand side of (34), namely $\bar{U}_0(S)$, represents clearly the (leading order) propagation speed of the triple flame under adiabatic conditions, since it is equal to $U_0$ when $\kappa = 0$. Introducing a rescaled heat loss coefficient and (leading order) propagation speed in the form

$$\chi \equiv \frac{\kappa}{\bar{U}_0^2} \qquad \text{and} \qquad V_0 \equiv \frac{U_0}{\bar{U}_0}, \tag{35}$$

respectively, we find that

$$V_0 \exp\left(\frac{\chi}{V_0^2}\right) = 1. \tag{36}$$

Equation (36) is well known to represent the propagation speed of a planar flame subject to volumetric heat losses (under assumptions similar to those adopted in this paper, see, e.g. [15]). A plot of the function $V_0(\chi)$ is provided in figure 4; it has two branches, with the lower one being unstable to one-dimensional disturbances. At the turning point, which characterizes extinction conditions, $V_0$ and $\chi$ have the critical values $V_{0\mathrm{crit}} = e^{-1/2}$ and $\chi_{\mathrm{crit}} = (2e)^{-1}$, respectively. Thus, we have a simple dependence of $U_0$ on $\kappa$ and $S$ of the form

$$U_0(\kappa, S) = \bar{U}_0(S) V_0\left(\frac{\kappa}{\bar{U}_0^2(S)}\right).$$

With $U_0$ now being known, we can reuse equation (31) to determine $f_0'$, and thus the flame shape to first approximation. This is illustrated in figure 5 for the case corresponding to $S = 1$. It is seen that an increase in the heat loss coefficient results in an increased curvature of the flame front and a reduction in its transverse and longitudinal extent (i.e. the $y$-interval over which the flame exists is reduced). This observation is easily explained by writing (31) in the form

$$\tilde{S}_L \exp\left(\frac{\tilde{\kappa}}{\tilde{S}_L^2}\right) = 1 \qquad \text{with } \tilde{S}_L = \frac{S_{L0}}{\bar{S}_L} \quad \text{and} \quad \tilde{\kappa} = \frac{\kappa}{\bar{S}_L^2},$$

which has no solution, $\tilde{S}_L(y)$, unless $\tilde{\kappa}(y) \leqslant (2e)^{-1}$. This inequality determines the range of values of $y$ over which the flame front can be described. For example, in the case $S = 1$, for

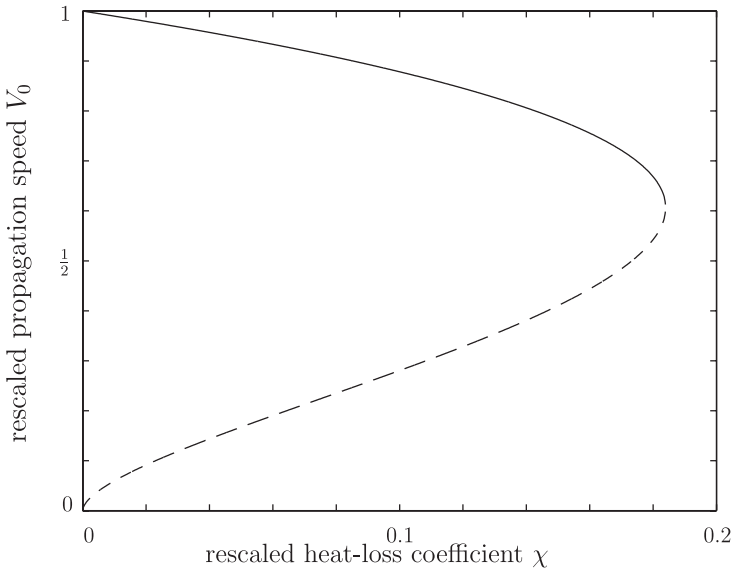


**Figure 4.** Rescaled propagation speeds $V_0$ for rescaled values of the heat loss $\chi$.

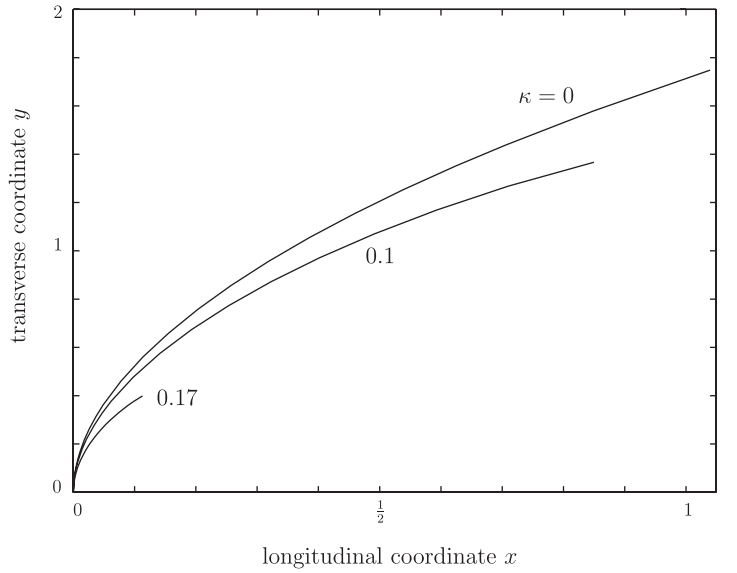


**Figure 5.** Flame shape $x = f(y)$ in the case $S = 1$.

which $\bar{S}_L^2 = (1 + 2|y|/\sqrt{\pi})\exp(-2|y|/\sqrt{\pi})$ from (12), (13) and (31), this range is $[-y_e, y_e]$, with $y_e$ being determined by the relation

$$\kappa = (2e)^{-1}\left(1 + \frac{2y_e}{\sqrt{\pi}}\right)\exp\left(-\frac{2y_e}{\sqrt{\pi}}\right).$$

This implies that $y_e$ decreases from $\infty$ to 0 as $\kappa$ is increased from 0 to the critical value $\kappa_{crit} = (2e)^{-1}$, suggesting that the flame front experiences total extinction when its burning

portion has become negligibly small. More generally, using (35) and (36), it is found that total extinction occurs for any value of $S$ when $\kappa$ exceeds $\kappa_{\rm crit} = (2e)^{-1}\bar{U}_0^2$.

Finally, for later reference, we evaluate $f''(y^*)$ by differentiating (31) with respect to $y$ and taking the limit $y \to y^*$. We thus obtain

$$f_0''(y^*) = \left[2\left(1 - \frac{2\kappa}{U_0^2}\right)\right]^{-1/2} \times \begin{cases} \gamma_{\rm F} & S \leqslant 1, \\ \gamma_{\rm O} & S \geqslant 1, \end{cases} \tag{37}$$

which can be expressed in terms of $S$ using (12) and (13) and which shows that the curvature of the flame front increases with $\kappa$. It can be noted that (37) implies that $f_0''(y^*) \to \infty$ as $2\kappa/U_0^2 \to 1$; in view of (34) this occurs when $\kappa$ approaches the critical extinction value $\kappa_{\rm crit} = (2e)^{-1}\bar{U}_0^2$. Near this point the asymptotic results must be expected to become innacurate.

### *3.3. The solution at the next approximation*

The results of the previous section provide a leading order description of the flame, in particular with regard to the propagation speed, $U$. To obtain a better description, we carry out the asymptotic analysis to the next order in $\epsilon$. If the operator L is defined by

$$\mathrm{L} \equiv 2f_0' f_1' \frac{\partial^2}{\partial\zeta^2} - f_0'' \frac{\partial}{\partial\zeta} - 2f_0' \frac{\partial^2}{\partial y \partial\zeta}, \tag{38}$$

then the governing equations in the inner region are

$$\begin{aligned}
&U_0 \frac{\partial\theta_1}{\partial\zeta} - (1 + f_0'^2)\frac{\partial^2\theta_1}{\partial\zeta^2} = \mathrm{L}(\theta_0) - U_1 \frac{\partial\theta_0}{\partial\zeta}, \\
&U_0 \frac{\partial h_1}{\partial\zeta} - (1 + f_0'^2)\frac{\partial^2 h_1}{\partial\zeta^2} = \mathrm{L}(h_0 + l_{\rm F}\theta_0) - U_1 \frac{\partial h_0}{\partial\zeta} + l_{\rm F}(1 + f_0'^2)\frac{\partial^2\theta_1}{\partial\zeta^2} - \kappa\theta_1, \\
&U_0 \frac{\partial k_1}{\partial\zeta} - (1 + f_0'^2)\frac{\partial^2 k_1}{\partial\zeta^2} = \mathrm{L}(k_0 + l_{\rm O}\theta_0) - U_1 \frac{\partial k_0}{\partial\zeta} + l_{\rm O}(1 + f_0'^2)\frac{\partial^2\theta_1}{\partial\zeta^2} - \kappa\theta_1.
\end{aligned} \tag{39}$$

These are to be solved for $\zeta \neq 0$, subject to the jump conditions

$$\begin{aligned}
&[\theta_1] = [h_1] = [k_1] = 0, \\
&\left[\frac{\partial h_1}{\partial\zeta}\right] = -l_{\rm F}\left[\frac{\partial\theta_1}{\partial\zeta}\right], \qquad \left[\frac{\partial k_1}{\partial\zeta}\right] = -l_{\rm O}\left[\frac{\partial\theta_1}{\partial\zeta}\right], \\
&\left[\frac{\partial\theta_1}{\partial\zeta}\right] = \left(\frac{\sigma_1}{2} + \frac{(\mu_1 - \sigma_1)/4}{1 + (\mu_0 - \sigma_0)/2} - \frac{f_0' f_1'}{1 + f_0'^2}\right)\left[\frac{\partial\theta_0}{\partial\zeta}\right],
\end{aligned} \tag{40}$$

at the reaction sheet, located at $\zeta = 0$.

Downstream of the reaction sheet, it is found that $\theta_1$ must be zero so as to be bounded as $\zeta \to \infty$ and to match with (21). We thus have from (39), after eliminating exponentially growing terms

$$\begin{aligned}
\theta_1 &= 0, \\
h_1 &= \hat{h}_1 + \frac{\kappa}{U_0^2}(f_0'' + U_1)\zeta, \\
k_1 &= \hat{k}_1 + \frac{\kappa}{U_0^2}(f_0'' + U_1)\zeta \qquad \text{for } \zeta \geqslant 0\,,
\end{aligned} \tag{41}$$

where $\hat{h}_1$ and $\hat{k}_1$ are independent of $\zeta$ and are as yet undetermined.

Solving for $\theta_1$ in the unburnt gas, it is found that

$$\theta_1 = \frac{\alpha}{U_0}\left[U_1 - 2f_0' f_1'\alpha + f_0'' - 2\frac{f_0'^2 f_0''}{1+f_0'^2}\alpha\zeta\right]\zeta\exp(\alpha\zeta) \qquad \text{for } \zeta \leqslant 0, \tag{42}$$

after using the matching requirement $\theta_1 \to 0$ as $\zeta \to -\infty$, and the continuity requirement $\theta_1 = 0$ at $\zeta = 0$. We shall not need the explicit solutions for $h_1$ and $k_1$ below. We now integrate equation (39) from $\zeta = -\infty$ to $\zeta = 0^-$ to obtain

$$\begin{aligned}
&(1+f_0'^2)\left[\frac{\partial\theta_1}{\partial\zeta}\right] = I_\theta - U_1,\\
&U_0\hat{h}_1 = I_h + l_{\mathrm{F}} I_\theta + \kappa G,\\
&U_0\hat{k}_1 = I_k + l_{\mathrm{O}} I_\theta + \kappa G,
\end{aligned} \tag{43}$$

after using (28)–(29), (40)–(41) and the matching condition that $\theta_1$, $h_1$ and $k_1$ and their derivatives with respect to $\zeta$ must vanish as $\zeta \to -\infty$. In (43), we have introduced the quantities

$$I_\theta = \int_{-\infty}^{0} \mathrm{L}(\theta_0)\,\mathrm{d}\zeta, \qquad I_h = \int_{-\infty}^{0} \mathrm{L}(h_0)\,\mathrm{d}\zeta, \qquad I_k = \int_{-\infty}^{0} \mathrm{L}(k_0)\,\mathrm{d}\zeta$$

and

$$G = \frac{1+f_0'^2}{U_0^2}(U_1 + f_0'') + \frac{2U_1}{\alpha U_0} - \int_{-\infty}^{0}\theta_1\,\mathrm{d}\zeta.$$

These can be evaluated from (28)–(29) and (42), hence

$$\begin{aligned}
U_0\hat{h}_1 &= -l_{\mathrm{F}} f_0'' + \frac{4\kappa(1+f_0'^2)}{U_0^2}\left[f_0'' - U_0\frac{f_0' f_1'}{1+f_0'^2} + 3\frac{f_0'^2 f_0''}{1+f_0'^2} + U_1\right],\\
U_0\hat{k}_1 &= -l_{\mathrm{O}} f_0'' + \frac{4\kappa(1+f_0'^2)}{U_0^2}\left[f_0'' - U_0\frac{f_0' f_1'}{1+f_0'^2} + 3\frac{f_0'^2 f_0''}{1+f_0'^2} + U_1\right],\\
U_1 &= -f_0'' + U_0\frac{f_0' f_1'}{1+f_0'^2} + \frac{\sigma_1}{2}U_0 + \frac{(\mu_1-\sigma_1)/4}{1+(\mu_0-\sigma_0)/2}U_0.
\end{aligned} \tag{44}$$

The system of three equations (44) contains four unknowns, $\hat{h}_1$, $\hat{k}_1$, $U_1$ and $f_1'$. However, it is possible to determine directly the perturbation in flame velocity, $U_1$, by applying (44) at the leading edge of the flame, $y^*$, where $f_0'(y^*) = 0$. Thus, using (19), we obtain

$$U_1\left(1 - \frac{2\kappa}{U_0^2}\right) = -f_0''(y^*)\left[\widetilde{L}(y^*) - \frac{2\kappa}{U_0^2}\right], \tag{45}$$

where

$$\tilde{L}(y) = \begin{cases} 1 + \dfrac{l_{\mathrm{F}}}{2} - \dfrac{l_{\mathrm{F}} - l_{\mathrm{O}}}{4(1+((\gamma_{\mathrm{F}}+\gamma_{\mathrm{O}})/2)y)} & (y \geqslant 0),\\[2ex] 1 + \dfrac{l_{\mathrm{O}}}{2} - \dfrac{l_{\mathrm{O}} - l_{\mathrm{F}}}{4(1-((\gamma_{\mathrm{F}}+\gamma_{\mathrm{O}})/2)y)} & (y \leqslant 0). \end{cases}$$

Since $y^*$ and $f_0'(y^*)$ are given by (33) and (37), we obtain

$$U_1 = -\frac{1+(\gamma_{\mathrm{O}}/(\gamma_{\mathrm{F}}+\gamma_{\mathrm{O}}))(l_{\mathrm{F}}/2) + (\gamma_{\mathrm{F}}/(\gamma_{\mathrm{F}}+\gamma_{\mathrm{O}}))(l_{\mathrm{O}}/2) - (2\kappa/U_0^2)}{\sqrt{2}\left(1-2\kappa/U_0^2\right)^{3/2}} \times \begin{cases}\gamma_{\mathrm{F}} & S \leqslant 1,\\ \gamma_{\mathrm{O}} & S \geqslant 1.\end{cases} \tag{46}$$

We note that (46) breaks down as $2\kappa/U_0^2 \to 1$, which occurs when $\kappa$ approaches the critical extinction value $\kappa_{\rm crit} = (2e)^{-1}\bar{U}_0^2$, as discussed just after equation (37). Thus (46) is not expected to be valid in near-extinction conditions.

At this stage, a two-term approximation, $U \sim U_0 + \epsilon U_1$, is available for the propagation speed from (34) and (46). This is the main result we have been seeking. It is seen that $U_0$ depends on $S$ and $\kappa$, and that $U_1$ depends on $S$, $\kappa$ and the reduced Lewis numbers, $l_{\rm F}$ and $l_{\rm O}$. For example, for the case where $S = 1$ (to be considered in the numerical study below) we find, using (12), (13), (34) and (46), that $U_0$ and $U_1$ are given by

$$U_0 \exp\left(\frac{\kappa}{U_0^2}\right) = 1 \qquad \text{and} \qquad U_1 = -\frac{1 + l_{\rm F}/4 + l_{\rm O}/4 - 2\kappa/U_0^2}{\left(1 - 2\kappa/U_0^2\right)^{3/2}}\sqrt{\frac{2}{\pi}}. \tag{47}$$

A plot of $U = U_0 + \epsilon U_1$ versus $\kappa$ based on these expressions will be given later in figure 7, where it is compared with numerical results.

Before finishing this section, we briefly mention that additional information can be obtained from (44). For example, for the perturbation in the flame slope, $f_1'(y)$, we find

$$f_1'(y) = \frac{U_0 U_1 + U_0^2 C(y) f_0''(y)}{S_{L0}^2(y) f_0'(y)},$$

in which all quantities on the right-hand side are now known. Here, $S_{L0} \equiv U_0/(1 + f_0'^2)^{1/2}$ is given in (31) and (32) and

$$C(y) \equiv U_0^{-1}\left[\tilde{L}(y) - (1 + 4f_0'^2)\frac{2\kappa}{U_0^2}\right]\left[1 - \frac{2\kappa}{S_{L0}^2}\right]^{-1}.$$

Similarly, a two-term expansion for the local burning speed, $S_L$, is found to be

$$S_L \sim S_{L0}(y)[1 - \epsilon C(y) f_0''(y)],$$

with the second term in the bracket accounting for the combined effect of differential diffusion, curvature and heat loss.

Finally, for the temperature of the flame front, $\theta_{\rm fl}$ say, we find

$$\theta_{\rm fl} = \begin{cases} 1 - \dfrac{\gamma_{\rm F}}{\beta} y - \dfrac{2\kappa}{\beta S_{L0}^2} - \dfrac{l_{\rm F} + \kappa\tilde{C}(y)}{\beta U_0}\epsilon f_0''(y) & \text{(fuel-lean side),} \\ 1 + \dfrac{\gamma_{\rm O}}{\beta} y - \dfrac{2\kappa}{\beta S_{L0}^2} - \dfrac{l_{\rm O} + \kappa\tilde{C}(y)}{\beta U_0}\epsilon f_0''(y) & \text{(fuel-rich side),} \end{cases}$$

where $\tilde{C}(y) \equiv 4U_0 S_{L0}^{-2} C(y) - U_0^{-2}(1 + 4f_0'^2)$. The first term on the right-hand side of these expressions, equal to 1, is the flame temperature in the absence of heat loss and gradients in the fresh mixture, that is the adiabatic flame temperature of a planar stoichiometric flame. The second term, linear in $y$, describes the deviation of flame temperature for an infinitely thin flame ($\epsilon = 0$), resulting from the linear deviation of mass fractions and of temperature in the fresh mixture from their values at the upstream stoichiometric location as dictated by (11). The third term is the drop in temperature of such an infinitely thin locally planar flame associated with heat loss. The fourth term accounts for the coupling between flame curvature, differential diffusion and heat loss.

At this stage, the meaning of fuel-lean and fuel-rich sides can be made more precise. These are given to leading order by $y > 0$ and $y < 0$, respectively. To first order in $\epsilon$, they are given by $y > y_{\rm s}$ and $y < y_{\rm s}$, with $y_{\rm s}$ being the root of $h_0 + \epsilon h_1 = k_0 + \epsilon k_1$; hence

$$y_{\rm s} \sim \frac{l_{\rm O} - l_{\rm F}}{U_0(\gamma_{\rm F} + \gamma_{\rm O})}\epsilon f_0''(0).$$

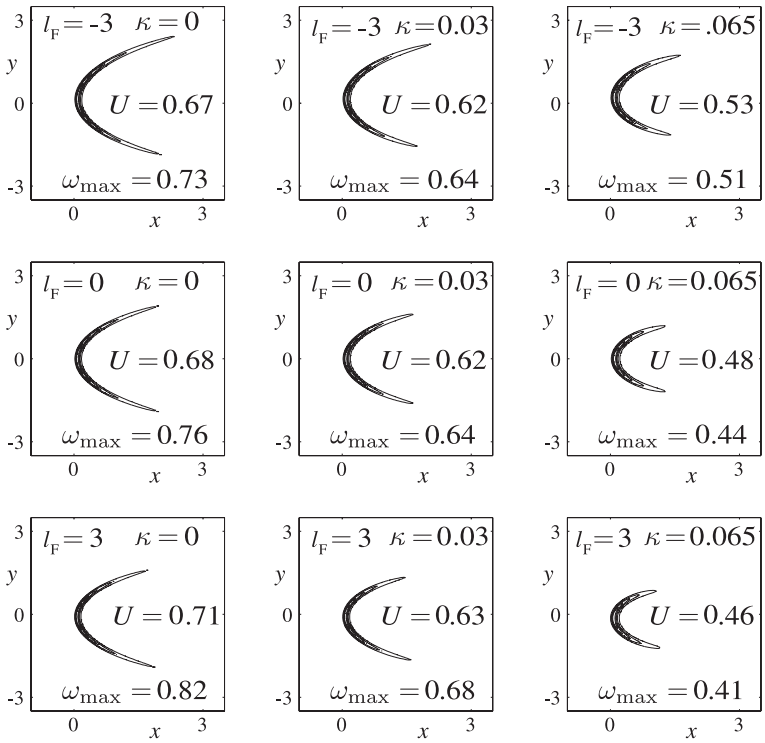


**Figure 6.** Reaction rate contours for $\epsilon = 0.1$.

Since $y_s$ is $O(\epsilon)$, it is clear that the two expressions for the flame temperature give the same result at $y = y_s$ within an error of $O(\epsilon^2)$. Finally, it can be noted that the expressions for $f_1'$, $S_L$ and $\theta_{fl}$ are valid only when the denominator of $C(y)$ is larger than zero, namely for $2\kappa/S_{L0}^2(y) < 1$. When this condition is violated, the flame is extinguished locally.

## 4. Numerical calculations and comparison with the asymptotic results

In this section, the asymptotic description above is complemented by and compared with numerical results. The numerical results will focus on assessing the validity of the asymptotic predictions and will thus be restricted to low strain situations allowing however for differential diffusion and for a wide variation of the heat loss intensity from adiabatic to extinction conditions. In this respect they complement our previous publication [14], which was restricted to unity Lewis numbers and did not include any comparison with analytical results. As in [14], the problem (5)–(10) is solved numerically using the finite volume method combined with an algebraic multigrid solver. The dimensions of the computational domain are typically 10 times the mixing layer thickness in the $y$-direction and 100 times the planar laminar flame thickness in the $x$-direction. A non-uniform grid with typically 200 000 points is used. The calculations correspond to $\beta = 8$, $\alpha_h = 0.85$, $\mathrm{Le_O} = 1$ and $\eta_s = 0$ (or $S = 1$), with the values of other parameters to be indicated in each case.

We begin with figure 6, which provides an overall picture of the combined influence of differential diffusion and heat loss for a fixed value of the strain rate, $\epsilon = 0.1$. Plotted are reaction rate contours for the selected values of $l_F$ and $\kappa$ indicated in each subfigure, with $l_F$

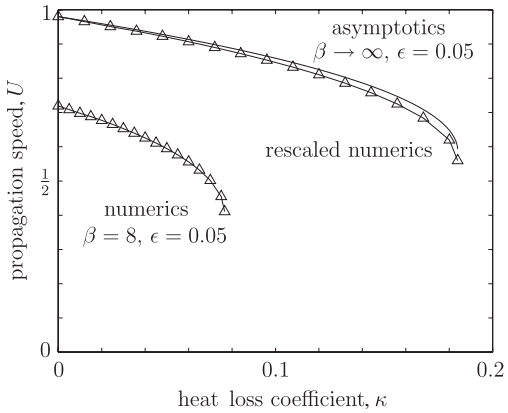


**Figure 7.** Propagation speed, $U$, as a function of the heat loss coefficient, $\kappa$, at the dimensionless strain rate $\epsilon = 0.05$.

being constant along the rows and increasing from top to bottom and $\kappa$ being constant along the columns and increasing from left to right. The contours are equidistributed between zero and the maximum value, $\omega_{\max}$, which is indicated along with the propagation speed, $U$, of the triple flame. We note, as we may expect and as suggested by the analytical study above, that for a fixed value of $l_{\mathrm{F}}$, the front curvature is stronger and the propagation speed is weaker in the presence of heat loss and that the flame is more sensitive to heat loss for larger values of $l_{\mathrm{F}}$. In particular, it is seen that the extent of the flame front in the transverse direction decreases as $\kappa$ is increased, in agreement with figure 5, which is based on the analytical results in the limit $\epsilon \to 0$. We also note that the trailing diffusion flame is absent for all the cases under discussion, except when $\kappa = 0$; in this latter case the diffusion flame is however too weak (when its burning rate is compared with that of the premixed front) and thus does not feature in the contour plot. The absence of the diffusion-flame tail at the low value of epsilon adopted here is mainly associated with the fact that the rate of heat generation by the chemical reaction decreases as the strain rate (or reactant supply) is decreased, leading to extinction whenever $\kappa \neq 0$. Extinction does not occur however when $\kappa = 0$ in the Burke–Schumann limit, as $\epsilon \to 0$, since the flame temperature tends then to unity (its adiabatic value), although the reaction rate becomes vanishingly small.

A first comparison between the asymptotic and numerical results, addressing the dependence of the propagation speed on $\kappa$, is illustrated in figure 7 for the case $\epsilon = 0.05$. The asymptotic results use the two-term expansion, $U = U_0 + \epsilon U_1$, given in (47) with $l_{\mathrm{F}} = 0$ (and $l_{\mathrm{O}} = 0$). Although the qualitative agreement is clear, we note a quantitative discrepancy that can be attributed to the finite activation energy used in the computations (see, e.g. [16]). More precisely, the numerics predict a lower value of $\kappa$ at extinction, $\kappa_{\mathrm{ext}}^{\mathrm{num}} \approx 0.08$, compared with the asymptotic value $\kappa_{\mathrm{ext}}^{\mathrm{asy}} = (2e)^{-1} \approx 0.184$; lower values of $U$ are similarly predicted, e.g. the numerical value for $U$ corresponding to $\kappa = 0$, say $\hat{U}$, is found to be equal to $\hat{U}^{\mathrm{num}} \approx 0.72$, while the asymptotic value is $\hat{U}^{\mathrm{asy}} = 1 - \epsilon\sqrt{2/\pi} \approx 0.960$. However, a simple linear rescaling of the numerical results ($\kappa \mapsto \kappa\, \kappa_{\mathrm{ext}}^{\mathrm{asy}}/\kappa_{\mathrm{ext}}^{\mathrm{num}}$, $U \mapsto U\, \hat{U}^{\mathrm{asy}}/\hat{U}^{\mathrm{num}}$) shows that the overall variation of the rescaled numerics compares very well with the asymptotics, even under near-extinction conditions.

A second comparison between the asymptotic and numerical predictions is carried out in figure 8 for $\epsilon = 0.1$ and three values of $l_{\mathrm{F}}$. Here the triangles, circles and squares pertain to cases with $l_{\mathrm{F}} = 0$, $l_{\mathrm{F}} = 3$ and $l_{\mathrm{F}} = -3$, respectively. The dashed curves are based on

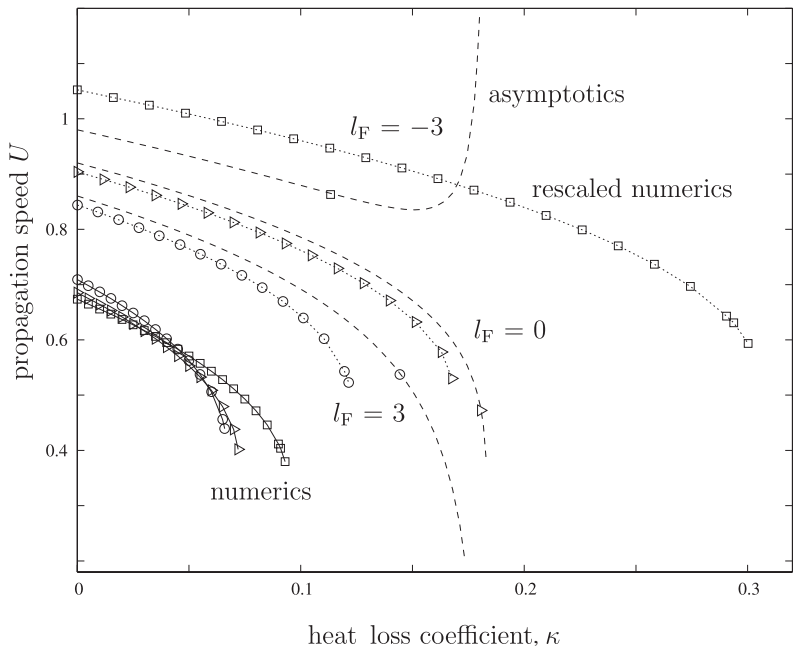


**Figure 8.** Propagation speed, $U$, as a function of the heat loss coefficient, $\kappa$, for $\epsilon = 0.1$. The $l_F = 0$ cases are characterized by triangles, the $l_F = 3$ cases by circles and the $l_F = -3$ cases by squares. The solid curves correspond to the numerical results, the dotted curves to rescaled numerics as described in the text, and the dashed curves to asymptotics.

the asymptotic formula (47). Of course, the validity of this formula becomes questionable under near-extinction conditions; this is in particular the case for the portion of the curve corresponding to $l_F = -3$, where $U$ would be predicted to increase with increased heat loss, $\kappa$, something that is unlikely to be realized physically. The solid curves represent the numerical results, and the dotted curves are the same results rescaled so as to achieve a better quantitative agreement with the asymptotics. Again, the quantitative discrepancy can be attributed to the finite value of $\beta$ used in the numerical study. Here, our rescaling is slightly different from the one used in figure 7 and is based on the flame speed, $S_L^{0,\mathrm{num}}$, and the extinction heat loss coefficient, $\kappa_{\mathrm{ext}}^{0,\mathrm{num}}$, of the planar unstretched flame; these are obtained numerically and differ significantly from the theoretical values, $S_L^{0,\mathrm{asy}} = 1$ and $\kappa_{\mathrm{ext}}^{0,\mathrm{asy}} = 0.184$, valid in the asymptotic limit $\beta \to \infty$ [1]. More precisely, we use the rescaling: $\kappa \mapsto \kappa\kappa_{\mathrm{ext}}^{0,\mathrm{asy}}/\kappa_{\mathrm{ext}}^{0,\mathrm{num}}$, $U \mapsto U\, S^{0,\mathrm{asy}}/S^{0,\mathrm{num}}$.

A good agreement between the asymptotic and the rescaled numerical results can then be observed, except for the low Lewis number case $l_F = -3$, not only for $\kappa > 0.3$. The discrepancy in the latter case occurs in fact even in the absence of heat losses and can be explained as follows. According to (47) with $l_O = 0$ and $\kappa = 0$, $U = U_0 + \epsilon U_1$ becomes an increasing function of $\epsilon$ (or the strain rate) when $l_F$ is below the critical value $l_{F,\mathrm{crit}} = -4$;

[1] For the value $\beta = 8$ adopted in the numerics, $(S_L^{0,\mathrm{num}}, \kappa_{\mathrm{ext}}^{0,\mathrm{num}})$ are found to be equal to $(0.76, 0.080)$ when $l_F = 0$, $(0.84, 0.10)$ when $l_F = 3$, and $(0.64, 0.057)$ when $l_F = -3$. Although one way of improving the quantitative agreement is to use higher values of $\beta$ in the numerics, at the expense of increasing the computational cost, especially in the two-dimensional case, a prohibitive increase in $\beta$ is needed for a quantitative agreement within a few per cent, e.g. even for $\beta = 20$ we find $(S_L^{0,\mathrm{num}}, \kappa_{\mathrm{ext}}^{0,\mathrm{num}}) = (0.88, 0.12)$ when $l_F = 0$, which are still significantly different from the asymptotic values. Similar discrepancies are described in [16].

strictly speaking the very existence of the planar flame is questionable for $l_F < l_{F,crit}$ (for sufficiently small $\epsilon$) since the cellular instability is then to be expected. We emphasize that $l_{F,crit} = -4$ is predicted in the asymptotic limit $\beta \to \infty$. Numerically the critical value $l_{F,crit}^{num}$ (below which $U$ becomes an increasing function of $\epsilon$, for small $\epsilon$) turns out to be slightly above $-3$, for the value of $\beta = 8$ as adopted here. This is evidenced, e.g. by the fact that, for $l_F = -3$, the initial point on the rescaled numerical curve, is above one (i.e. when $\kappa = 0$, the propagation speed is higher than that of the planar unstretched flame), while the asymptotic formula predicts a value below one. In short, the unsatisfactory comparison between the asymptotics and numerics in the latter case is due to the fact that $l_F$ in this case falls between the asymptotic critical value, $l_{F,crit}$, and the computed value, $l_{F,crit}^{num}$. Although use of higher values of $\beta$ can reduce the range of such discrepancies, we shall not pursue this issue any further.

## Conclusions

We have presented an analytical study of the effect of volumetric heat loss on triple flames in a counterflow configuration that is constrained to be two-dimensional in nature. The model was formulated using the thermo-diffusive approximation, a single-step Arrhenius reaction and a linear volumetric heat loss term. Analytical results were obtained for the propagation speed, the local burning speed and the shape of the triple flame front in the asymptotic limit of a large activation energy and weak strain rate. These were complemented with and compared with an extensive set of numerical results, with the main focus being on assessing the validity of the asymptotic predictions in low strain situations, both for unit and non-unit Lewis numbers. As a whole, the study provides significant insight into the combined effects of strain, heat loss, composition gradients and non-unit Lewis numbers, which seems to be lacking in the literature. Although restricted to a simple flow configuration, the findings do provide a valuable first step in deriving Markstein-type relationships between the local burning speed and local flame stretch in non-homogeneous non-adiabatic mixtures.

## References

[1] Phillips H 1965 *10th Symp. (Int.) on Combustion* (Pittsburg, PA: The Combustion Institute) p 1277
[2] Ohki Y and Tsuge S 1986 *Dynamics of Reactive Systems: Part I* ed J R Bowen *et al Prog. Astronaut. Aeronaut.* **105** 233
[3] Dold J W 1989 *Combust. Flame* **76** 71–88
[4] Hartley L J and Dold J W 1991 *Combust. Sci. Technol.* **80** 23
[5] Liñán A 1994 *Combustion in High Speed Flows* ed J Buckmaster *et al* (Boston, MA: Kluwer) p 461
[6] Kioni P N, Rogg B, Bray C and Liñán A 1993 *Combust. Flame* **95** 276–90
[7] Buckmaster J and Matalon M 1988 *22nd Symp. (Int.) on Combustion* (Pittsburg, PA: The Combustion Institute) pp 1527–35
[8] Ruetsch G R, Vervisch L and Liñán A 1995 *Phys. Fluids* **7** 1447–54
[9] Daou J and Liñán A 1998 *Combust. Theory Modelling* **2** 449–77
[10] Shay M L and Ronney P D 1998 *Combust. Flame* **112** 171
[11] Nayagam V and Williams F A 2002 *J. Fluid Mech.* **458** 219
[12] Kurdyumov V and Matalon M 2002 *Proc. Combust. Inst.* **29** 45–52
[13] Daou R, Daou J and Dold J 2003 *Combust. Theory Modelling* **7** 221–42
[14] Daou R, Daou J and Dold J 2002 *Proc. Combust. Inst.* **29** 1559–64
[15] Joulin G and Clavin P 1976 *Acta Astronaut.* **3** 223
[16] Dold J W, Thatcher R W and Shah A A 2003 *Combust. Theory Modelling* **7** 109–27